SUPPORTING INFORMATION

Detecting Order and Lateral Pressure at Biomimetic Interfaces Using a Mechanosensitive Second-Harmonic-Generation Probe

Giuseppe Licari,[a] *Joseph S. Beckwith,*[a] *Saeideh Soleimanpour,*[b] *Stefan Matile,*[b] *and Eric Vauthey**[a]

a) Department of Physical Chemistry, b) Department of Organic Chemistry, University of Geneva, 30 quai Ernest-Ansermet, CH-1211 Geneva 4, Switzerland.

1. Additional spectroscopic measurements **S2**

2. Additional computational results **S9**

3. Analysis of the polarization-resolved SSHG data **S11**

4. Additional experimental details **S15**

References **S16**

1. Additional spectroscopic measurements

Stationary electronic absorption and fluorescence spectroscopy

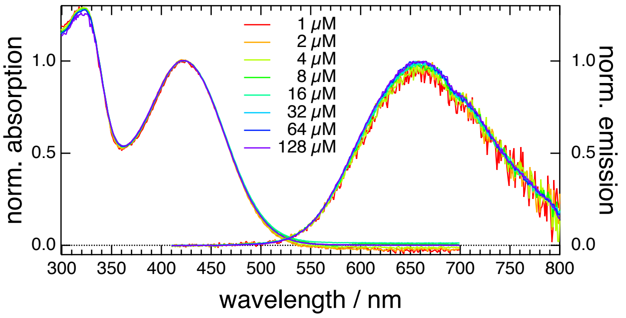

Figure S1. Absorption and emission spectra of **1** in DMSO at different concentrations.

Additional stationary SSHG spectra

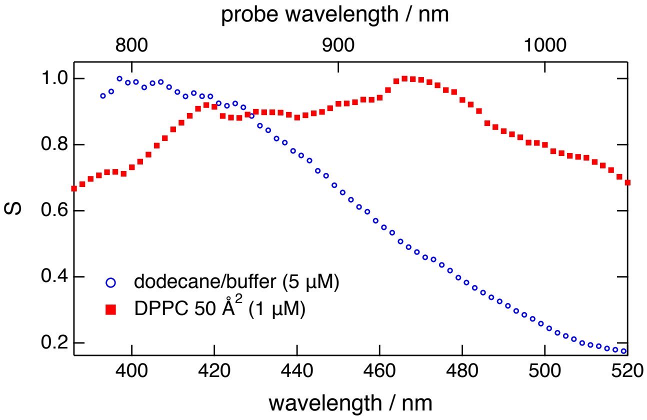

Figure S2. SSHG spectra, $S(\lambda)$, of **1** at the dodecane/buffer and dodecane/DPPC/buffer interfaces..

Time-resolved broadband fluorescence

In FLuorescence UP-conversion Spectroscopy (FLUPS), the whole fluorescence spectrum is recorded as a function of time with femtosecond time resolution, allowing a direct observation of the excited-state dynamics.

The FLUPS measurements were performed with a setup similar to that reported by Zhang et al.[S1] In brief, excitation was carried out with 100 fs pulses at 400 nm generated by frequency-doubled output of a standard 1 kHz Ti:Sapphire amplified system. The pump intensity on the sample was below 1 mJ·cm^{-2}. The gate pulses were at 1340 nm and were produced using an optical parametric amplifier (TOPAS C, Light Conversion). Detection of the up-converted spectra was performed with a CCD camera (Andor, DV420A-BU). The full width at half maximum of the cross correlation of the gate pulse with the solvent Raman signal was approximately 170 fs. Corrected time-resolved emission spectra were obtained by calibration with secondary emissive standards as described in ref. S2. Time-resolved emission spectra were recorded on a linear time-step range from -1 to 2 ps, followed by a logarithmic time-step range from 2 to 1000 ps. The crystal orientation was set to orientation B in the nomenclature of Gerecke et al.,[S3] to increase the spectral coverage.

In a previous work,[S4] FLUPS measurements with a compound similar to **1** (structure **2** in ref. S4) were reported. The results in non-polar solvents showed a distinct shift of the fluorescence band towards lower energy within a few picoseconds after excitation. In the absence of dipolar solvent relaxation, this shift was assigned to the planarization of the molecule. As shown in Figure S3, a similar bathochromic shift occurs with a solution of **1** in DMSO within the first 10 ps. Bandshape analysis allows extraction of the fluorescence peak shift as a function of time (Figure S5). The total peak shift corresponds to a stabilization energy of about 0.5 eV. This value agrees with that obtained from the DFT-calculated shift of the excitation energy upon going from a dihedral angle of 90° to 140° (0.44 eV).

The time evolution of the fluorescence intensity was analyzed globally using either a sum of exponential functions or assuming a series of successive exponential steps.[S5] The first approach gives Decay-Associated Emission Spectra (DAES), whereas the second yields Evolution-Associated Emission Spectra (EAES). Five exponentials (hence five successive steps) were necessary to reproduce the whole broadband emission recorded within a 1 ns time window (Figure S3 and Table S1). The DAES and EAES obtained from this analysis are shown in Figure S4. The first three EAES reveal that the emission band shifts from around 530 nm to 600 nm within the first 10 ps. The three corresponding time constants can be associated with structural relaxation (i.e. planarization) as well as solvent/vibrational relaxation. As all these processes occur on overlapping timescales, a more precise assignment is not possible. Elimination of solvent relaxation by performing FLUPS measurements in non-polar solvents was not possible because of the very limited solubility of **1**.

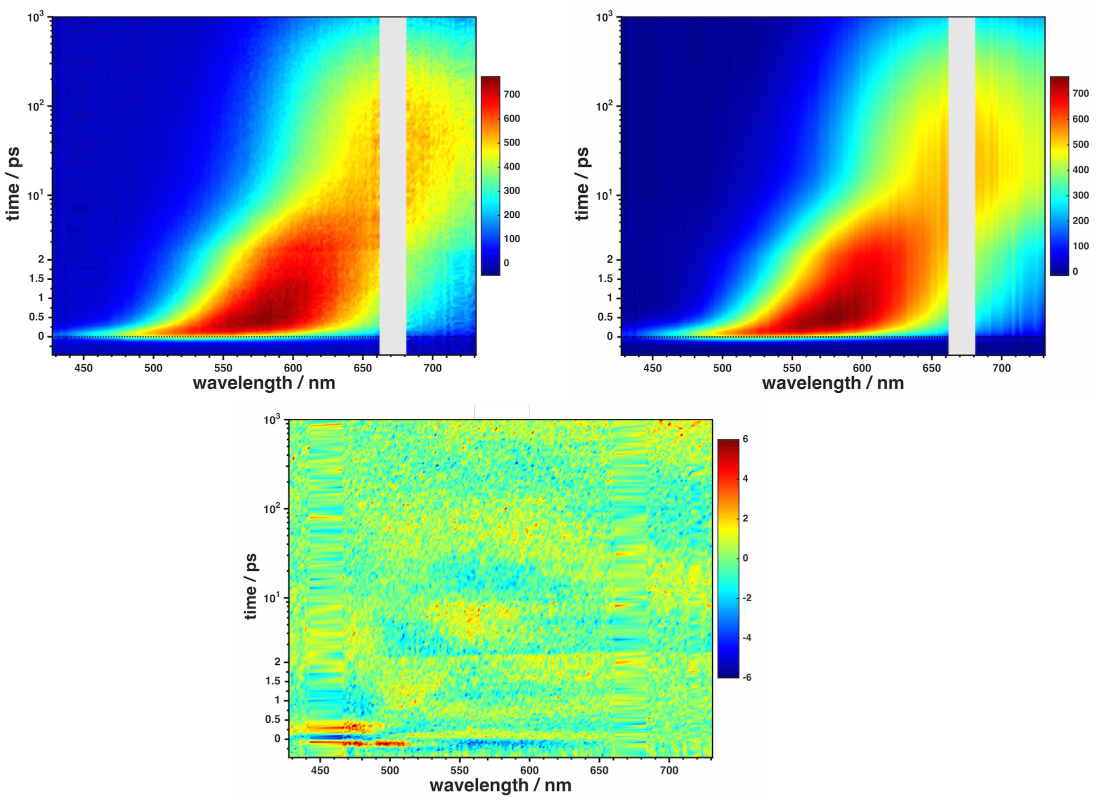

Figure S3. Time-resolved fluorescence measured upon 400 nm excitation of **1** in DMSO (top left), best global fit (top right) and residual (bottom). Five exponentials were needed to properly reproduce the data (the time constants are reported in Table S1). The gray rectangle removes the spectral region where fluorescence overlaps with the third harmonic of the gate pulse used for up-conversion.

Table S1. Time constants (in picoseconds) obtained from multiexponential weighted global analysis to the FLUPS data. The exponential functions were convolved with a Gaussian function that reproduces the instrument response function (IRF). The lifetime τ_5 was fixed to the long lifetime obtained from time-correlated single-photon-counting measurements.

τ_1	τ_2	τ_3	τ_4	τ_5	***IRF*** (FWHM)
< IRF	0.97 ± 0.1	4.9 ± 0.6	116 ± 10	1470 (fixed)	0.22 ± 0.01

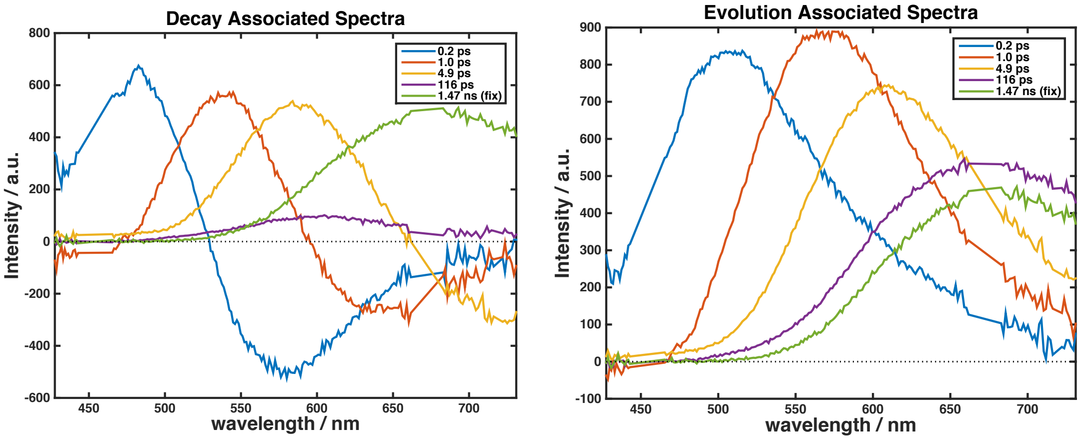

Figure S4. Decay Associated (DAES, left) or Evolution Associated (EAES, right) emission spectra obtained from the global analysis of the FLUPS data in DMSO.

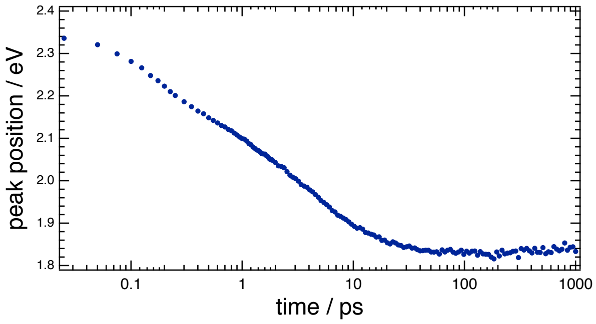

Figure S5. Time evolution of the peak position obtained from the fit of a log-normal function to the fluorescence spectra recorded in DMSO.[S2, 6]

Transient absorption measurements

The femtosecond transient absorption (TA) setup has been described previously.[S7] Excitation was carried out at 400 nm and the instrument response function had a full width at half-maximum of ~100-300 fs as derived from optical Kerr effect measurements in DMSO. The sample was excited with ~1 mJ·cm^{-2} pump intensity. It was saturated and then bubbled with nitrogen during the measurement to constantly refresh the excitation volume. Changes in the sample concentration due to degradation and/or solvent evaporation were negligible as judged from absorption spectrum before and after the experiment.

TA spectra recorded with **1** in DMSO are shown in Figure S6. The data were analyzed similarly to the broadband emission by using a global analysis with either the sum of five exponential functions or assuming a series of five successive exponential steps. The resulting Decay-Associated Difference absorption Spectra (DADS) and Evolution-Associated Difference absorption Spectra (EADS) together with the corresponding time constants are shown in Figure S7 and Table S2. These spectra point to a shift of the stimulated emission within the first few picoseconds, as observed for the time-resolved fluorescence. An intense excited-state absorption band overlaps with the stimulated emission, which makes it difficult to disentangle the various contributions to the excited-state relaxation. The ground-state bleach is present until the end of the measurement, in agreement with a nanosecond excited-state lifetime of **1**. The time profile of the TA intensity at 415 nm is reported in Figure 4 in the main text. This profile, together with the EADS, suggests that the dynamics at this wavelength mostly reflects the recovery of the ground-state population. The small increase of the bleach during the first ~10 ps is probably due to the contribution of the overlapping stimulated emission.

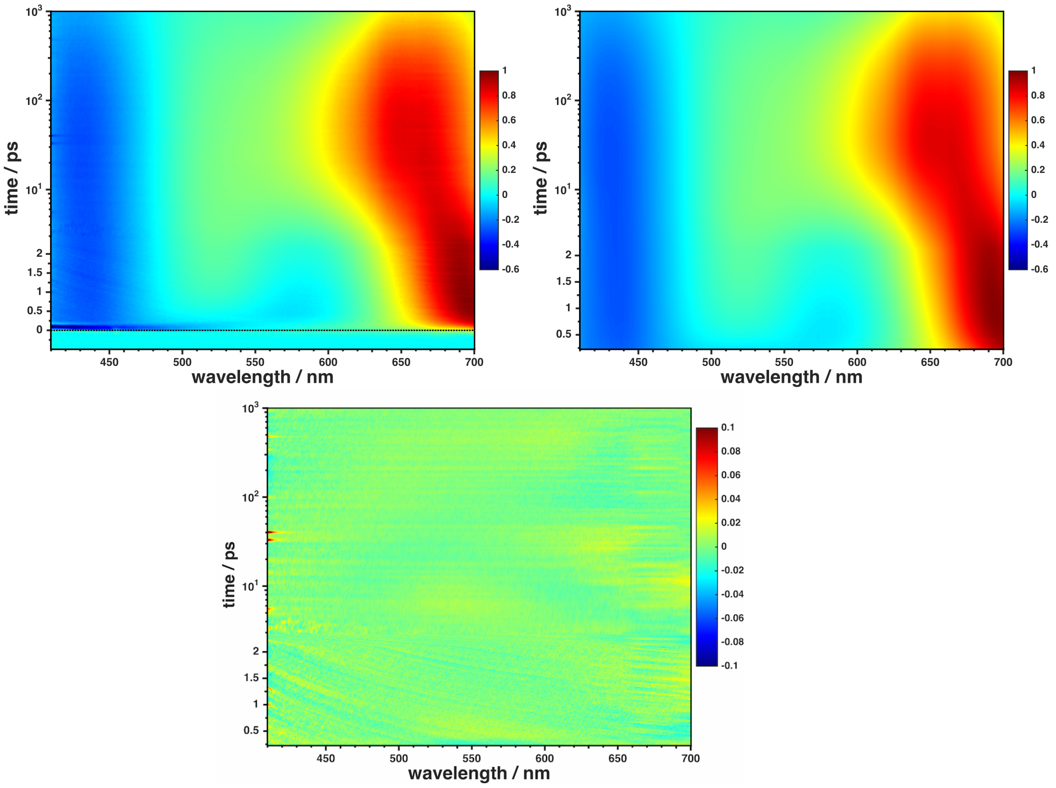

Figure S6. Transient absorption measured after 400 nm excitation of **1** in DMSO (top left), best multiexponential fit (top right) and residual (bottom). Five exponentials were needed to properly reproduce the data (the time constants are reported in Table S2).

Table S2. Time constants (in picoseconds) obtained from multiexponential fit to the transient absorption data. The exponential functions were fitted to the data starting from 0.2 ps.

τ_1	τ_2	τ_3	τ_4	τ_5
0.46 ± 0.1	2.1 ± 0.3	9.3 ± 0.5	770 ± 15	> 1.5 ns

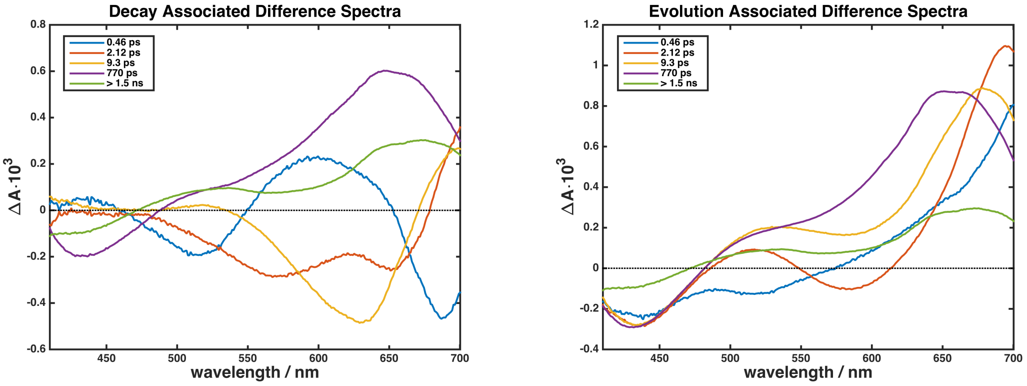

Figure S7. Decay Associated Difference (DADS, left) or Evolution Associated Difference (EADS, right) spectra obtained from global analysis of the transient absorption data in DMSO.

Time-resolved surface second harmonic generation

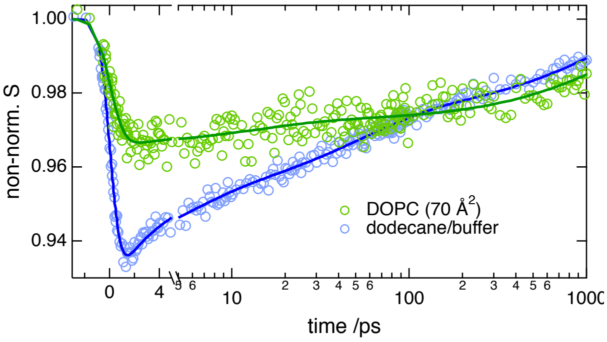

Figure S8. TR-SSHG profiles measured at 415 nm with **1** at the dodecane/buffer and dodecane/DOPC/buffer interfaces after 515 nm excitation using p/p polarization for probe and signal fields. The non-normalized signal intensity corresponds to the square root of the SHG intensity with pump on divided by the SHG intensity with pump off. The time axis is linear up to 5 ps and logarithmic afterward. The solid lines are best multiexponential fits to the data.

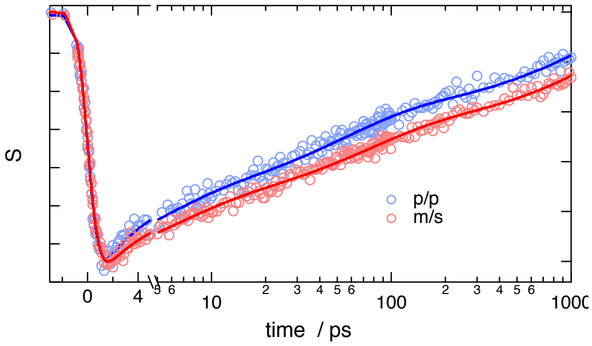

Figure S9. TR-SSHG profiles, $S(t)$, measured at 415 nm with **1** at the dodecane/buffer interface after 515 nm excitation using p/p and m/s polarization for probe and signal fields. The time axis is linear up to 5 ps and logarithmic afterward. The solid lines are best multiexponential fits to the data. The main difference between the two profiles is in the relative amplitude of the slow component (τ_3), which amounts to 0.36 with p/p polarization and 0.42 with m/s polarization.

Table S3. Time constants (in picoseconds) obtained from multiexponential weighted fit to the TR-SSHG data shown in Figure 4 and amplitude-averaged time constants. The exponential functions were convolved with a Gaussian function that reproduces the instrument response function (IRF). The time resolution of the TR-SSHG is around 1-2 ps.

interface	**τ_1 / ps**	**τ_2 / ps**	**τ_3 / ns**	**<τ> / ps**	***IRF***
dodecane/buffer	4.1 ± 1.1 (32%)	48 ± 11 (32%)	1.1 ± 0.3 (36%)	420 ± 100	1.6 ± 0.1
dodecane/DOPC/buffer	13 ± 12 (21%)	-	1.6 ± 0.5 ns (79%)	1300 ± 330	2.2 ± 0.6

2. Additional computational results

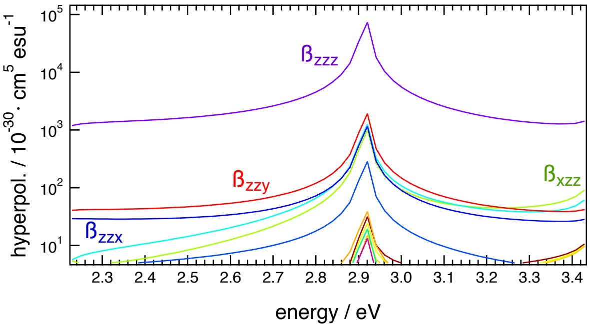

Figure S10. Calculated full frequency-dependent hyperpolarizability tensor elements (only the main elements are shown) of the analogue of **1** (Figure S12) with a dihedral angle of 123°. The tensor elements for different dihedral angles are similar with the exception of the resonantly enhanced maxima, which are shifted in energy. The sum of the real and imaginary parts is plotted and the most intense elements are indicated.

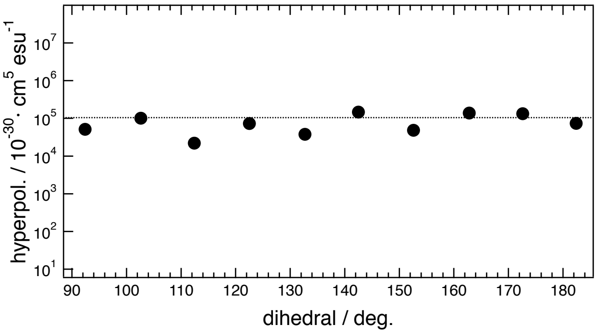

Figure S11. Total intrinsic quadratic hyperpolarizability (as defined in ref. S8) at the resonance maximum as a function of the dihedral angle. The fluctuation of the value is due to the numerical error associated with the calculation of the frequency-dependent hyperpolarizability near resonance.

In order to estimate the performance of **1** as an harmonophore, its calculated β was compared to that calculated using the same procedure for the ANEP chromophore (aminonaphthylethenylpyridinium), whose β is known from hyper-Rayleigh scattering measurements.[S9] For the calculations, all the substituents of the N atoms of ANEP were replaced by methyl groups. The out-of-resonance β value calculated for ANEP at 1064 nm (2.3 eV) amounts to $1.85 \cdot 10^{-27}$ cm^5 esu^{-1}, in good agreement with the experimental β value of $1.35 \cdot 10^{-27}$ cm^5 esu^{-1} measured at the same wavelength.[S9] On the other hand, the out-of-resonance β value calculated for **1** at 2.3 eV is $1.38 \cdot 10^{-27}$ cm^5 esu^{-1}. Thus, according to these calculations, the out-of-resonance β value of **1** is smaller by a factor 1.3 than that of ANEP. At resonance, this ratio amounts to 1.6.

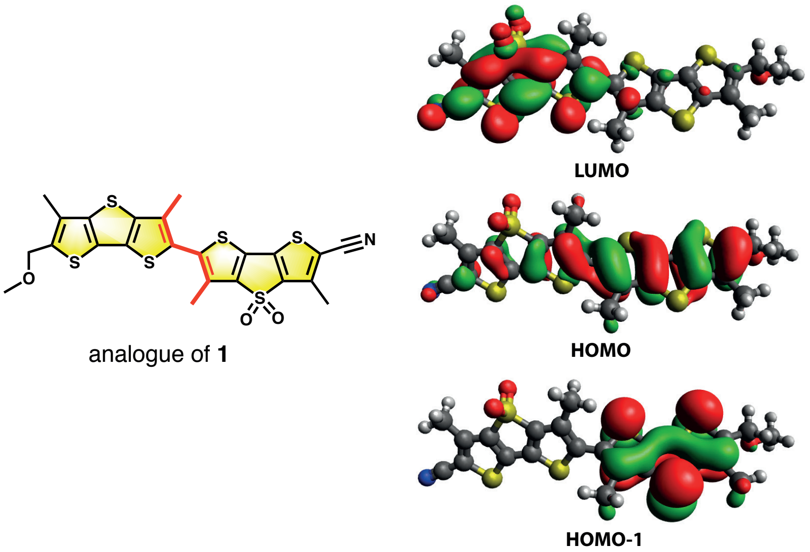

Figure S12. Analogue of **1** and its frontier molecular orbitals drawn at 0.02 a.u. isovalue. The first excited state is dominated by the HOMO – LUMO (61%) and HOMO-1 – LUMO (32%) transitions, pointing to a charge-transfer (CT) excitation. The mechanosensitive dihedral angle of the structure shown here amounts to 123°.

3. Analysis of the polarization-resolved SSHG data

The nonlinear SSHG intensity (I_{SSHG}) at frequency 2ω under total internal reflection condition can be expressed as:[S10, 11]

$$I_{SSHG} = \frac{\omega^2}{8\varepsilon_0 c^3} \frac{\left(\varepsilon_1^{2\omega}\right)^{1/2}}{\varepsilon_1^{\omega}\left(\varepsilon_m^{2\omega} - \varepsilon_1^{\omega}\sin^2\theta_1^{\omega}\right)} \left|\chi^{(2)}\right|^2 I_{pr}^2 \qquad \text{(S1)}$$

where $\varepsilon_{1,m}^{\omega}$ and θ_1^{ω} are the relative dielectric constants and the angle of incidence of the probe beam at ω, respectively. The subscripts *1* and *m* refer to the upper dodecane phase and the interface, respectively. The macroscopic nonlinear optical susceptibility, $\vec{\chi}^{(2)}$, is a second rank tensor containing 27 elements. For liquid interfaces, only seven non-zero elements, three of which being independent, have to be considered: $\chi_{ZZZ}^{(2)}$, $\chi_{ZXX}^{(2)} = \chi_{ZYY}^{(2)}$, and $\chi_{XXZ}^{(2)} = \chi_{XZX}^{(2)} = \chi_{YZY}^{(2)} = \chi_{YYZ}^{(2)}$, where the subscripts are the Cartesian coordinates in the laboratory frame, with *X* and *Y* being in the interfacial plane, and *Y* and *Z* being in the plane of incidence of the optical beams. The dependence of the SSHG intensity polarized at Γ on the polarization of the probe field, γ, is given by:

$$\begin{aligned} I_{SSHG}(\gamma,\Gamma) = C\Big| & a_1\chi_{XXZ}^{(2)}\sin 2\gamma\sin\Gamma + \left(a_2\chi_{XXZ}^{(2)} + a_3\chi_{ZXX}^{(2)}\right. \\ & \left. + a_4\chi_{ZZZ}^{(2)}\right)\cos^2\gamma\cos\Gamma + a_5\chi_{ZXX}^{(2)}\sin^2\gamma\cos\Gamma\Big|^2 I_{pr}^2 \end{aligned} \qquad \text{(S2)}$$

where the a_1-a_5 coefficients (listed in Table S4) are determined from the refractive indices of the different media and the angle of incidence. These coefficients were calculated as described in ref. [S10] using the following values:

$$n_{1,dod} = 1.42; \quad n_{2,wat} = 1.33; \quad n_m = 1.378$$

where n_m was calculated as the average of n_1 and n_2.[S12] Moreover, the frequency dependence of the refractive indices was neglected. The angle of incidence of the probe field was fixed experimentally at 70°, which satisfies the total internal reflection condition.

Table S4. Coefficients determined from the refractive indices of the different media and the angle of incidence.

Coefficients	*Real part*	*Imaginary part*
a_1	5.37972	-5.84029
a_2	0.05387	-0.0627639
a_3	-0.026935	0.0313819
a_4	4.86507	-5.66829
a_5	5.37972	-5.84029

The polarization-resolved SSHG measurements were carried out at three different output polarizations, namely Γ = 0° (*p*), 45° (*m*), and 90° (*s*), allowing the relative magnitude and sign of the three independent susceptibility elements to be extracted. The following expressions can be obtained from eq. (S2):

$$I_{SSHG}\left(\gamma,0^{\mathrm{o}}\right)\propto\left|\left(a_2\chi^{(2)}_{XXZ}+a_3\chi^{(2)}_{ZXX}+a_4\chi^{(2)}_{ZZZ}\right)\cos^2\gamma+a_5\chi^{(2)}_{ZXX}\sin^2\gamma\right|^2$$

$$I_{SSHG}\left(\gamma,45^{\mathrm{o}}\right)\propto\left|a_1\chi^{(2)}_{XXZ}\sin2\gamma+\left(a_2\chi^{(2)}_{XXZ}+a_3\chi^{(2)}_{ZXX}+a_4\chi^{(2)}_{ZZZ}\right)\cos^2\gamma+a_5\chi^{(2)}_{ZXX}\sin^2\gamma\right|^2$$

$$I_{SSHG}\left(\gamma,90^{\mathrm{o}}\right)\propto\left|a_1\chi^{(2)}_{XXZ}\sin2\gamma\right|^2$$

These three equations can be used in a least-squares curve-fitting analysis of the experimental data to obtain the relative magnitudes of the susceptibility elements.

The macroscopic second-order nonlinear susceptibility depends on the hyperpolarizability tensor $\overset{\leftrightarrow}{\beta}$ as:

$$\overset{\leftrightarrow}{\chi}^{(2)}=\frac{1}{\varepsilon_0}N\left\langle T\right\rangle\overset{\leftrightarrow}{\beta} \tag{S3}$$

where $\left\langle T\right\rangle$ is a transformation tensor (averaging over all the orientations) from the molecular to the laboratory frames. Dye **1** can be considered as a linear molecule with a strong charge-transfer character along the molecular axis, as confirmed by DFT calculations. In this case, one can assume that a single element of the hyperpolarizability tensor is dominating, the one aligned along the main molecular axis *z*, β_{zzz} (*z* being defined as the axis parallel to the transition dipole moment). In such a situation, the relations between the macroscopic susceptibility and microscopic hyperpolarizability simplify to:[S10]

$$\begin{gathered}\chi^{(2)}_{ZXX}=\chi^{(2)}_{XXZ}=\frac{1}{2}N\left\langle\sin^2\theta\cos\theta\right\rangle\beta_{zzz}\\ \chi^{(2)}_{ZZZ}=N\left\langle\cos^2\theta\right\rangle\beta_{zzz}\end{gathered} \tag{S4}$$

where θ is the tilt angle.

The orientation parameter, D, is a suitable combination of the aforementioned susceptibility elements in order to eliminate β_{zzz} and the surface concentration *N*, and, in this case, can be expressed as:[S10, 13, 14]

$$D=\frac{\left\langle\cos^3\theta\right\rangle}{\left\langle\cos\theta\right\rangle}=\frac{\chi^{(2)}_{ZZZ}}{\chi^{(2)}_{ZZZ}+2\chi^{(2)}_{ZXX}} \tag{S5}$$

In the case of an infinitely narrow distribution of the angles at the interface, i.e. a Dirac distribution, eq. (S5) simplifies to $D = \cos^2\theta$. Otherwise, a definite distribution has to be applied. Here, a Dirac distribution is assumed for simplicity and all the extracted values are listed in Table S5.

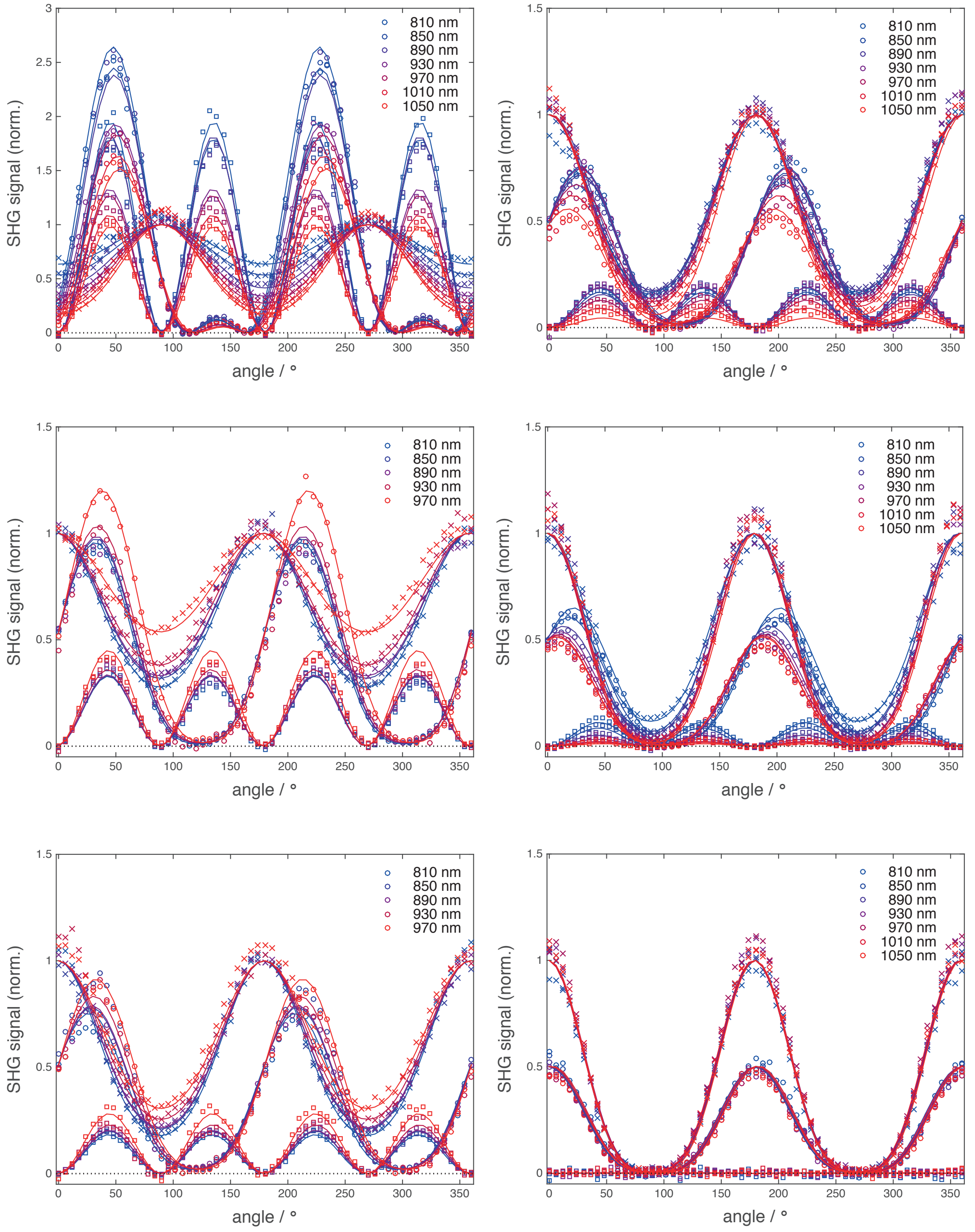

Figure S13. Polarization-resolved SSHG data. Left column: dodecane/buffer (top), dodecane/DOPC(70Å^2)/buffer (middle) and dodecane/DOPC(60Å^2)/buffer (bottom). Right column: dodecane/DPPC(90Å^2)/buffer (top), dodecane/DPPC(80Å^2)/buffer (middle) and dodecane/DPPC(70Å^2)/buffer (bottom). Three output polarization components (Γ) are reported: *square* = *s*, *cross* = *p* and *circle* = 45°. The best-fit curves are shown as solid lines. Each set of measurements was normalized to the maximum of the *p*-out fit curve.

Table S5. Results from the analysis of the polarization-resolved SSHG data of **1** at different wavelengths and mean molecular area. The global fit was performed on all three *p*, *s* and 45° polarization components. The errors were obtained from the weighted-fit procedure with 99% confidence interval using the inverse of the data standard error as weight and propagating the error through the various equations. The tilt angle θ was deduced assuming a Dirac distribution and a single dominant element of the β tensor.

	λ / nm	$\chi^{(2)}_{ZXX}/\chi^{(2)}_{XXZ}$	$\chi^{(2)}_{ZZZ}/\chi^{(2)}_{XXZ}$	***D***	θ /°
	dodecane/buffer				
	810	+0.740 ± 0.009	+0.593 ± 0.009	0.286 ± 0.003	57.7 ± 0.2
	850	+0.771 ± 0.015	+0.567 ± 0.012	0.269 ± 0.005	58.8 ± 0.3
	890	+0.766 ± 0.018	+0.494 ± 0.016	0.244 ± 0.007	60.4 ± 0.4
	930	+0.896 ± 0.019	+0.525 ± 0.013	0.227 ± 0.005	61.6 ± 0.3
	970	+0.916 ± 0.025	+0.482 ± 0.023	0.208 ± 0.008	62.9 ± 0.6
	1010	+0.991 ± 0.032	+0.461 ± 0.020	0.189 ± 0.008	64.3 ± 0.6
	1050	+1.043 ± 0.025	+0.435 ± 0.013	0.173 ± 0.005	65.4 ± 0.4
	1090	+1.106 ± 0.012	+0.374 ± 0.007	0.145 ± 0.002	67.7 ± 0.2
mma / Å^2	**dodecane/DOPC/buffer**				
70	**810**	+0.951 ± 0.020	+1.852 ± 0.030	0.493 ± 0.005	45.4 ± 0.3
	850	+1.016 ± 0.017	+1.849 ± 0.032	0.476 ± 0.004	46.4 ± 0.2
	890	+1.026 ± 0.023	+1.833 ± 0.033	0.472 ± 0.005	46.6 ± 0.3
	930	+1.063 ± 0.033	+1.770 ± 0.042	0.454 ± 0.007	47.6 ± 0.4
	970	+1.130 ± 0.027	+1.583 ± 0.035	0.412 ± 0.004	50.1 ± 0.2
60	**810**	+1.023 ± 0.026	+2.490 ± 0.046	0.549 ± 0.006	42.2 ± 0.3
	850	+1.060 ± 0.035	+2.384 ± 0.040	0.529 ± 0.008	43.3 ± 0.5
	890	+1.065 ± 0.023	+2.357 ± 0.030	0.525 ± 0.005	43.6 ± 0.3
	930	+1.091 ± 0.054	+2.222 ± 0.065	0.505 ± 0.011	44.7 ± 0.6
	970	+1.082 ± 0.047	+1.998 ± 0.056	0.480 ± 0.010	46.1 ± 0.6
mma / Å^2	**dodecane/DPPC/buffer**				
90	**810**	+0.97 ± 0.04	+2.46 ± 0.04	0.558 ± 0.009	41.6 ± 0.5
	850	+1.00 ± 0.02	+2.60 ± 0.04	0.566 ± 0.004	41.2 ± 0.2
	890	+1.09 ± 0.05	+2.70 ± 0.10	0.553 ± 0.006	42.0 ± 0.4
	930	+0.88 ± 0.05	+2.44 ± 0.05	0.582 ± 0.013	40.3 ± 0.7
	970	+1.00 ± 0.03	+2.96 ± 0.06	0.596 ± 0.005	39.5 ± 0.3
	1010	+1.08 ± 0.08	+3.52 ± 0.20	0.621 ± 0.012	38.0 ± 0.7
	1050	+1.20 ± 0.15	+5.04 ± 0.42	0.677 ± 0.020	34.7 ± 1.2
	1090	+0.93 ± 0.08	+4.55 ± 0.23	0.709 ± 0.015	32.7 ± 1.0
80	**810**	+1.06 ± 0.04	+3.19 ± 0.07	0.601 ± 0.008	39.2 ± 0.5
	850	+0.93 ± 0.05	+3.65 ± 0.11	0.663 ± 0.011	35.5 ± 0.6
	890	+1.07 ± 0.09	+4.71 ± 0.24	0.688 ± 0.014	34.0 ± 0.9
	930	+0.97 ± 0.07	+5.91 ± 0.30	0.753 ± 0.010	29.8 ± 0.7
	970	+1.08 ± 0.16	+7.12 ± 0.65	0.767 ± 0.020	28.9 ± 1.4
	1010	+1.02 ± 0.13	+8.04 ± 0.80	0.799 ± 0.014	26.7 ± 1.0
	1050	+1.22 ± 0.23	+9.97 ± 1.44	0.803 ± 0.020	26.3 ± 1.4
	1090	+0.71 ± 0.14	+5.70 ± 0.52	0.800 ± 0.030	26.6 ± 2.0
70	**810**	+2.3 ± 1.7	+47 ± 27	0.91 ± 0.04	17 ± 3.9
	850	+1.5 ± 0.5	+21 ± 6	0.88 ± 0.02	21 ± 2.1
	890	+7 ± 10	+114 ± 157	0.88 ± 0.02	20 ± 2.2
	930	+1.9 ± 0.9	+25 ± 11	0.87 ± 0.03	21 ± 2.4
	970	+1.7 ± 0.9	+23 ± 9	0.87 ± 0.02	21 ± 3.0
	1010	+2.2 ± 0.9	+28 ± 11	0.91 ± 0.03	22 ± 1.4
	1050	+1.0 ± 0.5	+22 ± 7	0.98 ± 0.04	17 ± 3.1

4. Additional experimental details

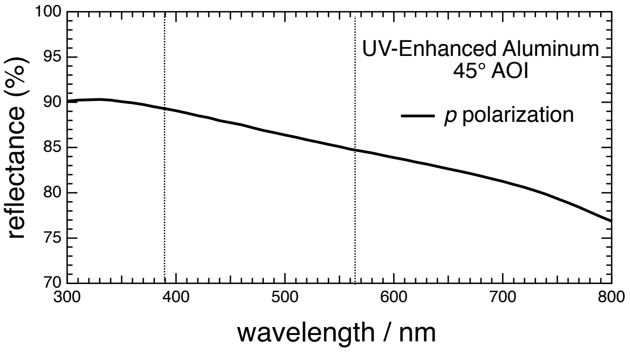

Figure S14. Reflectance of the mirror with UV-enhanced aluminum coating used as reference in the SSHG spectra measurements. The wavelength range used here is indicated by the two vertical dashed lines. The small decrease of the reflectance (about 5%) has a negligible effect on the shape of the SSHG spectra.

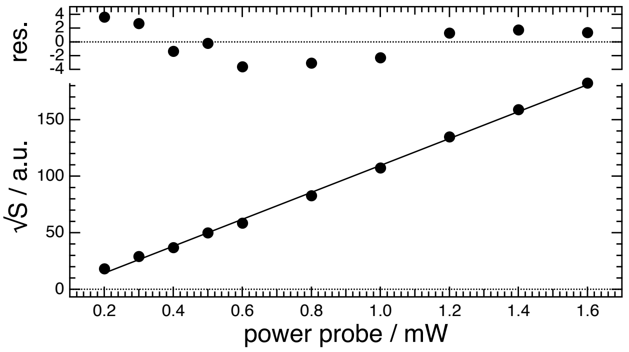

Figure S15. Linear dependence of the square root of the SSHG signal with respect to the average power of the probe light and best linear fit. The sample is **1** (10 µM) at the dodecane/buffer interface. The probe wavelength was set to 860 nm and 45° polarization. The *s* component of the SH signal was selected.

References

S1. X.-X. Zhang, C. Würth, L. Zhao, U. Resch-Genger, N. P. Ernsting and M. Sajadi, *Rev. Sci. Instrum.*, 2011, **82**, 063108.

S2. T. Kumpulainen, A. Rosspeintner and E. Vauthey, *Phys. Chem. Chem. Phys.*, 2017, **19**, 8815-8825.

S3. M. Gerecke, G. Bierhance, M. Gutmann, N. P. Ernsting and A. Rosspeintner, *Rev. Sci. Instrum.*, 2016, **87**, 053115.

S4. Q. Verolet, A. Rosspeintner, S. Soleimanpour, N. Sakai, E. Vauthey and S. Matile, *J. Am. Chem. Soc.*, 2015, **137**, 15644-15647.

S5. I. H. M. van Stokkum, D. S. Larsen and R. van Grondelle, *Biochim. Biophys. Acta, Bioenerg.*, 2004, **1657**, 82-104.

S6. P. F. Rusch and J. P. Lelieur, *Anal. Chem.*, 1973, **45**, 1541-1543.

S7. N. Banerji, G. Duvanel, A. Perez-Velasco, S. Maity, N. Sakai, S. Matile and E. Vauthey, *J. Phys. Chem. A*, 2009, **113**, 8202-8212.

S8. D. R. Kanis, M. A. Ratner and T. J. Marks, *Chem. Rev.*, 1994, **94**, 195-242.

S9. H. Li, G. Mao and K. D. Singer, *Proc. SPIE*, 2006, **6097**, 609705.

S10. P.-F. Brevet, *Surface Second Harmonic Generation*, Presses polytechniques et universitaires romandes, Lausanne, 1997.

S11. H. Nagatani, A. Piron, P.-F. Brevet, D. J. Fermin and H. H. Girault, *Langmuir*, 2002, **18**, 6647-6652.

S12. H. Wang, E. Borguet and K. B. Eisenthal, *J. Phys. Chem. B*, 1998, **102**, 4927.

S13. W.-K. Zhang, H.-F. Wang and D.-S. Zheng, *Phys. Chem. Chem. Phys.*, 2006, **8**, 4041-4052.

S14. Y. Rao, Y.-S. Tao and H.-F. Wang, *J. Chem. Phys.*, 2003, **119**, 5226.